

PAPER

10-Gbit/s Data Transmission Using 120-GHz-Band Contactless Communication with SRR Integrated Glass Substrate

Tomohiro KUMAKI[†], *Student Member*, Akihiko HIRATA^{†a)}, *Senior Member*, Tubasa SAIJO^{††}, *Nonmember*, Yuma KAWAMOTO^{††}, *Student Member*, Tadao NAGATSUMA^{††}, *Fellow*, and Osamu KAGAYA^{†††}, *Member*

SUMMARY We achieved 10-Gbit/s data transmission using a cutting-edge 120-GHz-band high-speed contactless communication technology, which allows seamless connection to a local area network (LAN) by simply placing devices on a desk. We propose a glass substrate-integrated rectangular waveguide that can control the permeability of the top surface to 120-GHz signals by contacting a dielectric substrate with the substrate. The top surface of the rectangular waveguide was replaced with a glass substrate on which split-ring resonators (SRRs) were integrated. The transmission loss of the waveguide with a glass substrate was 2.5 dB at 125 GHz. When a dielectric sheet with a line pattern formed on the contact surface was in contact with a glass substrate, the transmission loss from the waveguide to the dielectric sheet was 19.2 dB at 125 GHz. We achieved 10-Gbit/s data transmission by contacting a dielectric sheet to the SRR-integrated glass substrate.

key words: millimeter-wave wireless communications, bandstop filter, bandpass filter, metasurface

1. Introduction

The use of wireless local area networks (LAN) is expanding because they do not require wired cable connections and allow mobile terminals to freely connect to networks at various locations in a room. With increasing demands, wireless LANs are becoming increasingly faster, with transmission speeds of up to 6.9 Gbit/s for IEEE 802.11.ac [1] and 9.6 Gbit/s for IEEE 802.11.ax [2]. However, conventional wireless LAN technology limits the number of channels of access points and interchannel interference, resulting in unstable communication [3].

Sheet LAN is a potential candidate for addressing wireless LAN issues, including access concentration and interference at access points [4]. It is a new communication method that enables contactless connection with a LAN by simply placing mobile devices on a desk. A desk mounted with a LAN sheet is already in use. Sheet LAN transmits radio waves in the 5-GHz band by confining radio waves inside a dielectric sheet, achieving a maximum transmission speed of 300 Mbit/s [5]. One way to increase the data rate of the sheet LAN is to use a > 100-GHz-band millimeter-wave (MMW)

signal. Data transmissions of 10 Gbit/s and > 100 Gbit/s have been reported using 120 and 300 GHz wireless links, respectively [6]–[12].

In order to investigate how to boost the data rate of sheet LAN by utilizing a 120-GHz-band signal, we have been developing a 120-GHz-band sheet LAN technology [4]. In this study, a 120-GHz-band signal was transmitted in a dielectric sheet (Rogers RT/duroid 5880 [13]), and we achieved 10-Gbit/s data transmission. However, due to the MMW signal's high transmission loss [14], creating a 120-GHz band sheet LAN with a length of more than 1 m is challenging. For achieving a transmission distances of several meters, we investigate sheet LAN with hollow rectangular waveguides characterized by a low transmission loss of > 100-GHz-band signals. However, even if the receiver is in contact with the hollow rectangular waveguide, it cannot pick up radio signals traveling through it because the metal plates surrounding the waveguide's propagation route prevent it from doing so. We have proposed a hollow rectangular waveguide with split ring resonator (SRR)-integrated glass substrates in place of a metal plate on the top surface of the waveguide in order to achieve > 10-Gbps data transmission in a sheet LAN [15]. An SRR can produce the desired magnetic susceptibility (magnetic response), creating the necessary strong magnetic coupling with an applied electromagnetic field [16]–[20]. We developed 120-GHz-band radio wave absorbers and bandpass filters based on SRRs and successfully achieved 10 Gbit/s data transmission over 120-GHz-band wireless links using these devices [21]–[25]. The SRR integrated on the surface of the glass substrate reflected a 120-GHz-band signal traveling in the hollow waveguide, and the measured transmission loss of the glass-integrated rectangular waveguide was approximately 5 dB at 125 GHz. A portion of the millimeter-wave signal flowing in the waveguide was routed through the glass substrate to the dielectric sheet when a dielectric sheet was placed on the glass substrate. The transmission loss from the waveguide to the dielectric sheet was 21.2 dB at 125 GHz.

This paper presents a 10-Gbit/s data transmission with a 120-GHz-band close-proximity wireless link that employs a hollow rectangular waveguide with an SRR-integrated glass substrate. The transmission characteristics of a hollow rectangular waveguide with an SRR-integrated glass substrate were improved by increasing the precision of the mounting position on the glass substrate. Next, the transmission loss from the waveguide to the dielectric sheet in contact with

Manuscript received June 15, 2023.

Manuscript revised November 10, 2023.

Manuscript publicized February 8, 2024.

[†]Dept. of Information and Communication Systems Engineering, Chiba Institute of Technology, Narashino-shi, 275–0016 Japan.

^{††}Osaka University, Toyonaka-shi, 560–0043 Japan.

^{†††}Materials Integration Laboratories, AGC Inc., Yokohama-shi, 230–0045 Japan.

a) E-mail: hirata.akihiko@p.chibakoudai.jp

DOI: 10.1587/transele.2023ECP5024

the glass substrate was reduced by integrating line patterns on the contact surface of the dielectric sheet. We conducted a data transmission experiment using a hollow rectangular waveguide with an SRR-integrated glass substrate and a dielectric sheet with line patterns and succeeded in 10-Gbit/s data transmission.

2. Design of Hollow Rectangular Waveguide with Split Ring Resonator Integrated Glass Substrate

Figure 1 shows a conceptual diagram of the proposed sheet LAN system. A portion of the top surface of the hollow waveguide was removed, and a glass substrate was placed on the top surface to form the surface. The SRRs on the glass substrate reflect the 120-GHz-band MMW signal traveling in the hollow rectangular waveguide when no dielectric sheet is in contact with the glass substrate, as shown in Fig. 1 (a), which reduces the transmission loss from Port 1 to Port 2. When a dielectric sheet with line patterns is in contact with a glass substrate (Fig. 1 (b)), the resonant characteristics of the SRRs change, and a portion of the millimeter-wave signal propagating in the waveguide is guided through the glass substrate to the dielectric sheet.

Figure 2 shows schematics of the simulation models for full 3D electromagnetic (EM) simulations based on the finite element method (ANSYS HFSS). The size of the glass substrate was 7.714 mm × 3.6 mm, and the thickness of the glass substrate was 0.2 mm. The SRRs on the glass substrate were formed by a 5-μm-thick gold film. The manufacturing process was carried out according to the following procedures. First, Ti/Pd thin film was formed on the quartz substrate. After resist coating and resist pattern formation, SRR patterns are formed by gold plating. Next, after stripping the resist, the unnecessary Ti/Pd thin film is removed by etching. The gold conductivity was set to 41000000 siemens/m. The size of the hollow rectangular waveguide was 2 mm × 1 mm, and its length was 12.7 mm. Rogers RT/Duroid 5880 was used as a dielectric sheet. The width and thickness of the di-

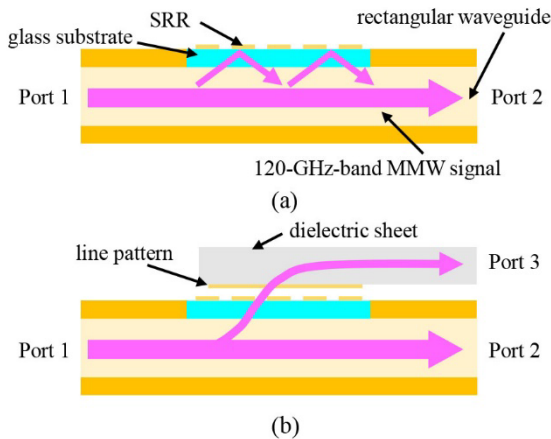


Fig. 1 Concept diagram of the LAN sheet system (a) when no dielectric sheet contacts the glass substrate, and (b) when a dielectric sheet contacts with the glass sheet.

electric sheet were 2.5 mm and 0.78 mm, respectively. Two cross-sections of the hollow rectangular waveguide were set up as ports 1 and 2. The section of the dielectric sheet on the same side as Port 2 was designated as port 3. Figure 3 (a) shows the SRR unit cell simulation model. We simulated the transmission loss of the hollow rectangular waveguide with an SRR-integrated glass substrate (S_{21}) for the case where no dielectric sheet is in contact with the dielectric sheet. SRR size parameters are as follows, unit cell size (a): 500 μm, SRR side length (b): 457 μm, capacitor length (c): 200 μm, capacitor gap (d): 21 μm, linewidth (e, L, w1): 87 μm, and gap between impedance and capacitor section (w2): 56 μm.

The dielectric sheet simulation model with added line patterns is shown in Fig. 4. This line pattern is designed to minimize the transmission loss from the rectangular waveguide to the dielectric sheet at 125 GHz when the dielectric sheet contacts the SRR integrated glass substrate. The distance from the edge of the dielectric sheet to the line patterns (f): 152 μm, the line width of the line patterns (g): 120 μm, the distance between the line patterns (h): 155 μm, and line pattern length: 7.5 mm.

Figure 5 shows the simulation results for the hollow waveguide models shown in Fig. 2. We simulated the S_{21}

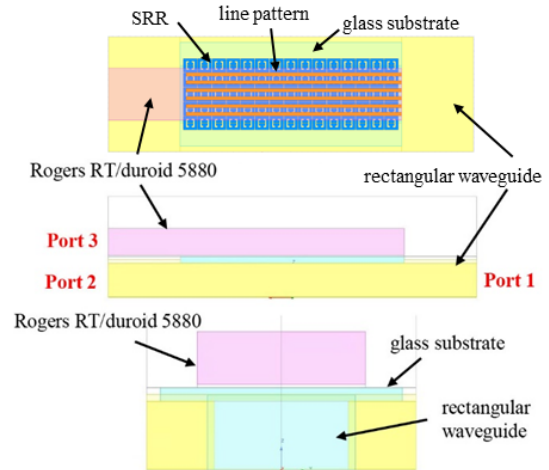


Fig. 2 Schematic diagrams of simulation models for the hollow rectangular waveguide with SRR integrated glass substrate.

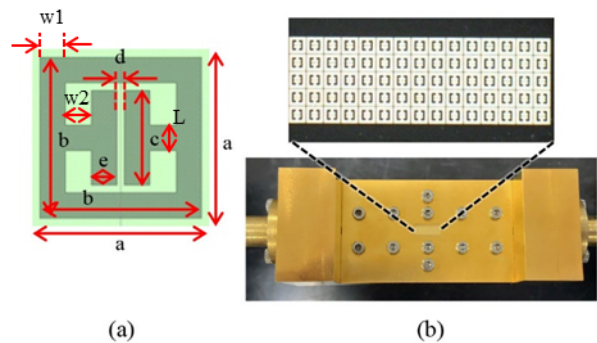


Fig. 3 (a) Schematic diagrams of SRR unit cell, (b) Photograph of SRR integrated glass substrate and waveguide module.

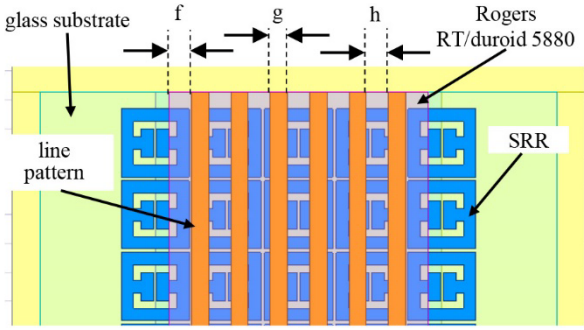


Fig. 4 Schematic diagram of simulation model of dielectric sheet with line pattern added.

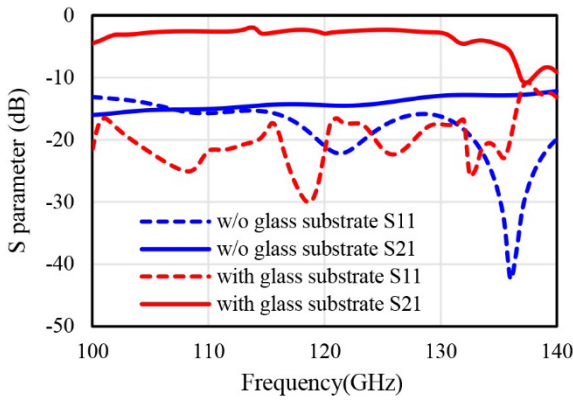


Fig. 5 Simulated S_{21} of the waveguide with SRR integrated glass substrate and without SRR integrated glass substrate.

characteristics of a hollow waveguide with and without a glass substrate on the top surface to investigate the impact of the glass substrate on the transmission properties of the hollow waveguide. S_{21} at 125 GHz was -2.31 dB when the glass substrate was integrated into the hole at the top surface of the hollow waveguide and -14.1 dB when the glass substrate was removed from the hole at the top surface of the hollow waveguide. Figure 6 (a) and 6 (b) show the simulated electric field distributions of the hollow waveguide with and without the glass substrate, respectively. In the electric field distribution of the model without the glass substrate in Fig. 6 (a), the 120-GHz-band signal leaks through the hole at the top surface of the waveguide. When the glass substrate is integrated into the hole at the top surface of the waveguide (Fig. 6 (b)), the 120-GHz-band signal leaking through the hole at the top surface of the waveguide is suppressed, and the transmission loss of the 120-GHz-band signal traveling inside the waveguide is also reduced. Based on these results, the integration of the glass substrate into the hole on the top surface of the waveguide reduces the transmission loss by approximately 11.79 dB.

We prototyped an SRR-integrated glass substrate and waveguide module with a hole of the same size as that of the glass substrate on the top surface of a hollow square waveguide. A glass substrate was attached to the holes. Figure 3 (b) shows a photograph of the prototype SRR-integrated

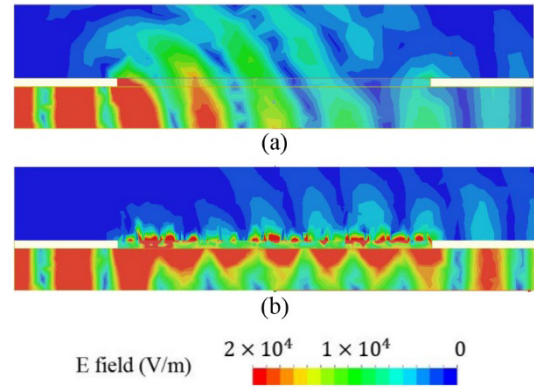


Fig. 6 (a) Simulation results of the electric field distribution without SRR integrated glass substrate. (b) Results of electric field distribution with an SRR integrated glass substrate.

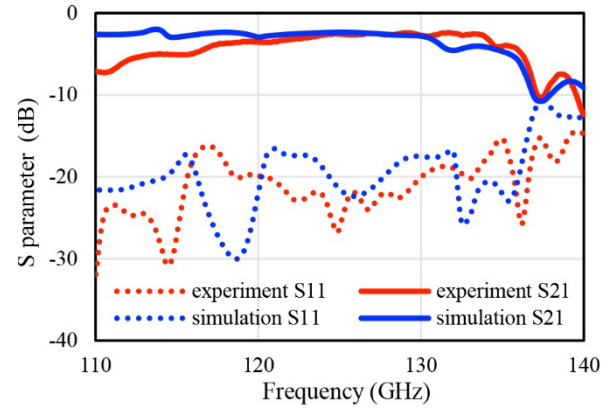


Fig. 7 Measured and simulated S_{11} and S_{21} of the waveguide with SRR integrated glass substrate.

glass substrate and the waveguide module on which the glass substrate was integrated. We measured the transmission loss of the waveguide module using a vector network analyzer (VNA). The frequency extenders of the VNA were connected to both waveguide ports of the waveguide module. Furthermore, we fabricated a waveguide module of the same size with no holes on top and measured its transmission loss. We calculated the difference in the transmission loss between these two modules and defined it as the transmission loss of the waveguide with the SRR-integrated glass substrate.

Figure 7 shows the simulated and measured transmission losses of the waveguide shown in Fig. 3 (a). The simulation results indicated that the transmission loss ranged from 2 to 5 dB at 110-130 GHz. The simulated S_{21} was -2.3 dB at 125 GHz. The measured S_{21} was -2.5 dB at 125 GHz, which is almost the same as the simulated S_{21} . The fluctuation of S_{21} from 115 to 135 GHz was 2.5 dB, and this frequency characteristic was sufficient for 10-Gbit/s data transmission with the ASK modulation scheme. In addition, the transmission losses were higher than those simulated results at 110-120 GHz. We believe that this difference arises from a gap or misalignment of the position of the SRR-integrated glass substrate during mounting.

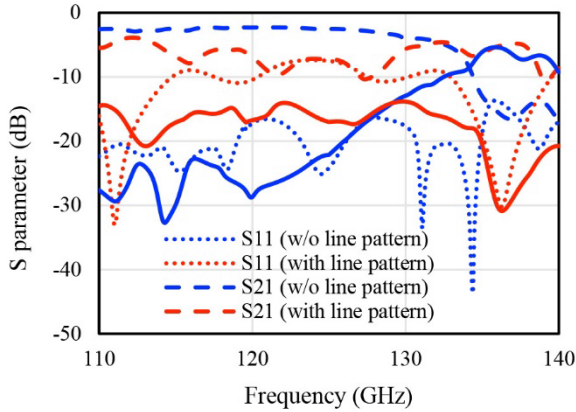


Fig. 8 Simulation results of S parameters with and without line patterns on the dielectric sheet in contact with the top of the waveguide.

3. Contactless Communication Using Dielectric Sheet

We investigated the possibility of extracting part of the millimeter-wave signal propagating in a hollow square waveguide and communicating with it by bringing the dielectric sheet into contact with a glass substrate placed on the top surface of the hollow square waveguide, as shown in Fig. 1 (b). Line pattern was added to the surface of the dielectric sheet in contact with the glass substrate to increase the proportion of 120-GHz-band signal that are guided to the dielectric sheet. Figures 8 and 9 shows the simulation results of S parameters and electric field distribution with and without the line pattern on the dielectric sheet, respectively. The simulation results showed that S_{21} was -2.52 dB and S_{31} was -22.12 dB at 125 GHz, when no line pattern was added to the dielectric sheet, and S_{21} was -7.25 dB and S_{31} was -16.99 dB at 125 GHz when a line pattern was added. The transmission loss tended to be lower at from 110 to 130 GHz when a line pattern was added. In addition, the electric field distribution in Fig. 9 shows that the magnitude of the signal guided to the dielectric sheet is stronger when the line pattern is added (Fig. 9 (c)) compared to that when no line pattern is added (Fig. 9 (a)) at 125 GHz. On the contrary, S_{31} with line pattern is lower than that without line pattern at over 130 GHz. We added the simulation results of electric field distribution at 125 GHz and 135 GHz as Fig. 9. When a dielectric sheet with no line pattern is in contact at 135 GHz (Fig. 9 (b)), a standing wave is generated at the glass substrate and the waveguide below it, and the 135 GHz band signal does not travel in the waveguide beyond the glass substrate. As a result, the leaked 135 GHz band signal is considered to have been guided to the dielectric sheet. On the other hand, the obvious standing wave was not observed at 135 GHz in case of the dielectric sheet without line pattern (Fig. 9 (d)). The presence or absence of these standing waves may be the cause of the difference in S_{31} at over 130 GHz. These results indicate that adding a line pattern to the dielectric sheet can guide 125 GHz signals to the dielectric sheet side.

Then, the transmission loss from the waveguide to the

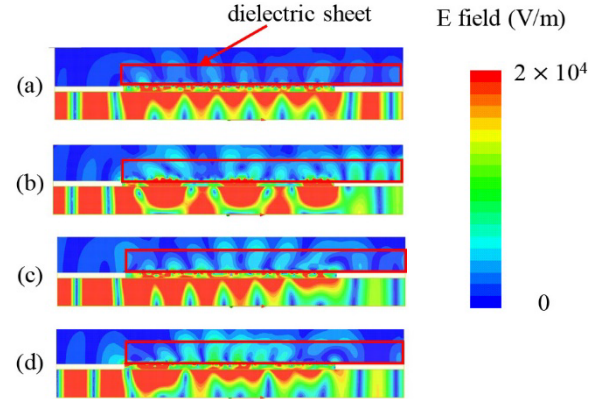


Fig. 9 (a, b) Simulation results of electric field distribution at 125 GHz (a) and 135 GHz (b) when line patterns are not formed on dielectric sheets. (c, d) Simulation results of the electric field distribution at 125 GHz (c) and 135 GHz (d) when the line patterns are formed on the dielectric sheet.

dielectric sheet was measured using a VNA. Figure 10 (a) shows a photograph of the measurement setup. A frequency extender was attached to the waveguide port of the waveguide module (Port 1), and another frequency extender was attached to the dielectric sheet (Port 3). The other waveguide port (Port 2) was terminated using a waveguide load. Rogers RT/Duroid 5880 was used as the dielectric sheet. The length, width, and thickness of the dielectric sheets were 100, 2.5, and 0.78 mm, respectively. One of the dielectric sheet's tips was tapered, and the tapered section was inserted into the frequency extender's waveguide to reduce transmission loss at Port 3. The other tip of the dielectric sheet is attached to the glass substrate. Figure 10 (b) shows a photograph of the tip of the dielectric sheet in contact with the glass substrate. A 100 mm-long dielectric sheet was connected to the waveguide port of the frequency extender by bending it such that it did not hit the waveguide module.

Figure 11 shows the measurement results of the transmission loss from the waveguide to the dielectric sheet in contact with and without the glass substrate on the hollow rectangular waveguide. The measured S_{31} at 125 GHz was -18.8 dB in case the line patterns are formed on the dielectric sheet, that was -23.7 dB in case there is no line pattern on the dielectric sheet. Therefore, the use of line pattern on the dielectric sheet decreases the transmission loss from the waveguide to the dielectric sheet by 4.9 dB.

It is important to evaluate the effect of bending the dielectric sheet on the transmission properties, because radiation loss occurs at the bending point of the dielectric sheet. Therefore, we measured the increase in the transmission loss of the dielectric sheet when it was bent. When the dielectric sheet was bent twice at 45 degree as shown in the photo in Fig. 10 (a), the increase in transmission loss of the dielectric sheet was approximately 3.5 dB at 125 GHz. The measured S_{31} at 125 GHz was -18.8 dB in case of the dielectric sheet with line pattern. Excluding the effect of bending of the dielectric sheet, the proportion of the 125 GHz signal guided into the dielectric sheet by contact is estimated to be

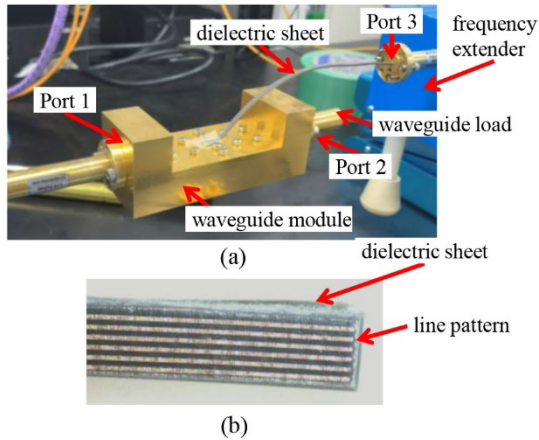


Fig. 10 (a) Photograph of the measurement setup for the transmission loss from the waveguide to the dielectric sheet. (b) Photograph of the tip of the dielectric sheet in contact with the glass substrate.

-15.3 dB. The fluctuation of S_{31} from 118 to 132 GHz was about 3.2 dB. These frequency characteristics are sufficient for 10-Gbit/s data transmission with the ASK modulation scheme.

The measurement results for S_{21} with and without the dielectric sheet in contact, are also shown in Fig. 11. The measurement results showed that S_{21} was -2.6 dB at 125 GHz when the dielectric sheet was not in contact with the glass substrate. On the other hand, measured S_{21} was -4.0 dB and S_{31} was -23.7 dB at 125 GHz, when no line pattern was formed to the dielectric sheet, and S_{21} was -5.1 dB and S_{31} was -17.7 dB at 125 GHz when a line pattern was formed. The measured transmission loss of a hollow rectangular waveguide with SRR integrated glass substrate increased by 1.4 dB when the dielectric sheet without line patterns was in contact with the glass substrate. This is because a portion of the MMW signal propagating in the hollow rectangular waveguide is guided by the dielectric sheet. On the other hand, the simulation results in Fig. 7 and 8 shows that the transmission loss increased by 0.2 dB by contacting the dielectric sheet without line pattern. We suppose that the difference of the increase in the transmission loss by contacting the dielectric sheet without line pattern between the experiment and the simulation can be attributed to the difference in the actual contact conditions between the glass and the dielectric sheet in the experiment and the simulation model.

The experimental result of S_{21} at is 1.5 dB larger than the simulation result of S_{21} in case the dielectric sheet without line pattern was in contact with the glass substrate. On the other hand, the experimental result of S_{21} is 2.2 dB smaller than the simulation result of S_{21} when the dielectric sheet with line pattern was in contact with the glass substrate. Moreover, the simulation and experimental results deviated significantly at frequencies above 130 GHz. The reason for this is thought to be the difference between the simulation model and the actual waveguide module and the differences in the contact conditions between the dielectric sheet and the

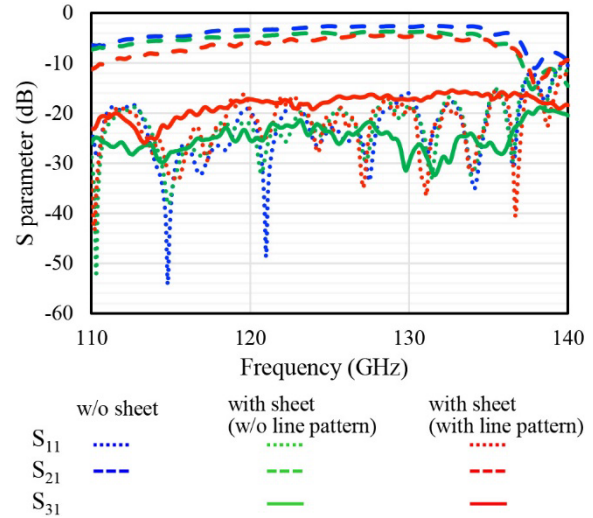


Fig. 11 Measurement results of the transmission loss from the waveguide to the dielectric sheet in contact with and without the glass substrate on the hollow rectangular waveguide.

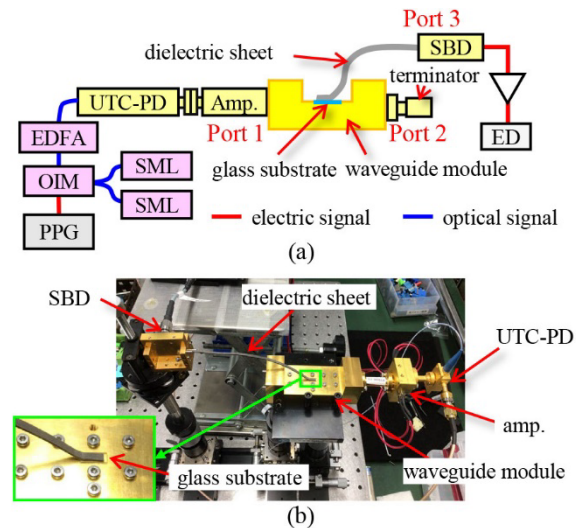


Fig. 12 (a) Schematic diagram and (b) photograph of experimental setup for data transmission characteristics of contactless communication.

glass substrate.

Finally, we verified the feasibility of data transmission through a dielectric sheet by contacting it with a glass-substrate-integrated hollow waveguide. Figures 12 (a) and 12 (b) show a schematic diagram and photograph of the experimental setup for data transmission characteristics of contactless communication using the dielectric sheet and hollow rectangular waveguide with an SRR-integrated glass substrate, respectively. The measurement setup for data transmission employed an ASK modulation scheme and envelope detection. The 120-GHz-band transmitter employs the optical generation of 120-GHz-band wireless signals based on two-mode beating. A 125-GHz-band optical subcarrier signal was generated by combining the output of two single-mode lasers (SMLs) and an optical intensity modulator

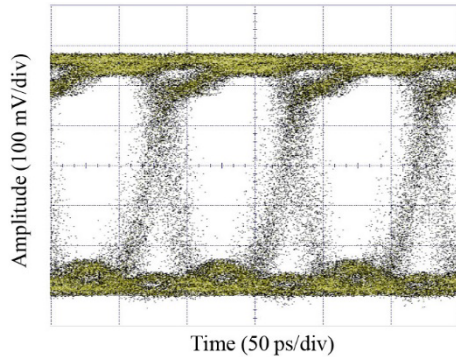


Fig. 13 Bit error rate (BER) characteristics of the wireless data transmission system at a data rate of 10.0 Gbit/s.

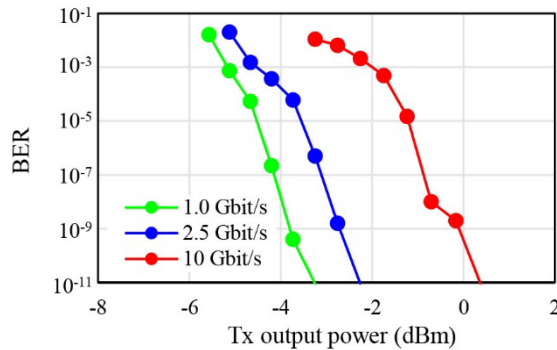


Fig. 14 Bit error rate (BER) characteristics of the wireless data transmission system at a data rate of 10.0 Gbit/s.

(OIM) modulated 125-GHz-band optical subcarrier signal using 10 Gbit/s data generated by a pulse pattern generator (PPG). The optical signal was amplified by an erbium-doped fiber amplifier (EDFA) and input into a uni-traveling carrier photodiode (UTC-PD) module [26]–[28], which converted the optical subcarrier signal to a 120-GHz-band MMW signal. The O/E-converted signal was amplified using a 120-GHz-band amplifier module [29], [30]. The waveguide output port of the amplifier module was connected to Port 1 of the waveguide module, as shown in Fig. 12(a). Port 2 of the waveguide module was terminated using a waveguide terminator. One of the tips of the 100-mm-long dielectric sheet was in contact with the glass substrate of the waveguide module, and the other tip of the dielectric sheet was inserted into the input port of the Schottky barrier diode (SBD) detector. The demodulated data signals are amplified using a baseband amplifier and fed into an error-rate detector (ED) or sampling oscilloscope. Figure 12 shows the eye pattern of the demodulated 10 Gbit/s data signal when the Tx output power was 0.5 dBm. Clear eye opening was observed. Figure 14 shows the dependence of the bit error rate (BER) characteristics of contactless communication on the Tx output power. Tx output power was measured at the output port of the 120-GHz-band amplifier module by connecting a power meter instead of the waveguide module. A bit error rate (BER) of below 10^{-11} was obtained with a transmission power of over -2.5 dBm at a data rate of 2.5 Gbit/s.

When the data rate was 10 Gbit/s, a BER below 10^{-11} was obtained with a Tx output power of 0.4 dBm. The BER characteristics at 10 Gbit/s characteristic is significantly degraded from those at 1.0 Gbit/s and 2.5 Gbit/s. As shown in Fig. 11, the transmission characteristics at the dielectric sheet contact are not flat at 118–132 GHz, which is the occupied bandwidth necessary for 10 Gbps data transmission. This fluctuation of the transmission characteristics causes the distortion of the 120-GHz-band wireless signal, which deteriorates the wireless data transmission characteristics at 10 Gbps. Thus, 10 Gbit/s data transmission through a dielectric sheet was achieved by contacting the dielectric sheet with a glass-substrate-integrated hollow waveguide.

4. Conclusions

We developed a hollow rectangular waveguide with an SRR-integrated glass substrate and applied it to a 120-GHz-band high-speed contactless communication. The SRR integrated on the surface of the glass substrate reflects a 120-GHz-band signal traveling in the hollow waveguide. The transmission loss of the hollow rectangular waveguide with the SRR-integrated glass substrate was 2.5 dB at 125 GHz. The transmission loss from waveguide to dielectric sheet at 125 GHz was 19.2 dB when the dielectric sheet was in contact with a glass substrate and had a line pattern established on the contact surface. We succeeded in 10-Gbit/s data transmission through a dielectric sheet by contacting the dielectric sheet with a glass-substrate-integrated hollow waveguide. These technologies enable high-speed contactless connections with LAN by simply placing mobile devices on a desk.

Acknowledgments

This study was partially supported by MEXT KAKENHI (grant number: JP 21H01328).

References

- [1] W.-S. Jung and Y.-B. Ko, "IEEE 802.11 ac based client centered indoor positioning system," 2016 IEEE Canadian Conference on Electrical and Computer Engineering (CCECE), Vancouver, BC, Canada, pp.1–4, 2016.
- [2] M.M. Hasan and M. Arifuzzaman, "VAQ-EDCA: Additional Video Access Queue Based EDCA Technique for Dense IEEE 802.11 AX Networks," 2019 International Conference on Computer, Communication, Chemical, Materials and Electronic Engineering (IC4ME2), pp.1–4, 2019.
- [3] J. Oh and Y.J. Chong, "Interference alignment for frequency selective fading channels in wireless local area network," 2017 Int. Conf. on Information and Communication Technology Convergence (ICTC), Jeju, Korea (South), pp.999–1001, 2017.
- [4] M. Ushio, F. Tokoro, A. Hirata, T. Higashimoto, Y. Uemura, T. Nagatsuma, N. Sekine, I. Watanabe, and A. Kasamatsu, "10-Gbit/s Data Transmission over Dielectric Sheet for 120-GHz-band Sheet LAN," 2020 International Symposium on Antennas and Propagation (ISAP), Osaka, Japan, pp.543–544, 2021.
- [5] <https://www.itoki-global.com/discover/history/>
- [6] A. Hirata, M. Harada, and T. Nagatsuma, "120-GHz wireless link using photonic techniques for generation, modulation, and emission

- of millimeter-wave signals,” *IEEE Journal of Lightwave Technology*, vol.21, no.10, pp.2145–2153, Oct. 2003.
- [7] A. Hirata, T. Kosugi, H. Takahashi, J. Takeuchi, H. Togo, M. Yaita, N. Kukutsu, K. Aihara, K. Murata, Y. Sato, T. Nagatsuma, and Y. Kado, “120-GHz-band wireless link technologies for outdoor 10-Gbit/s data transmission,” *IEEE Trans. Microw. Theory Tech*, vol.60, no.3, pp.881–895, March 2012.
- [8] A. Dogadaev, A.V. Lavrinenko, and I.T. Monroy, “Capacity analysis for high-speed terahertz wireless communications,” *Int. Conf. Infrared, Millimeter, and Terahertz Waves*, 2012.
- [9] J. Takeuchi, A. Hirata, H. Takahashi, N. Kukutsu, Y. Yamada, K. Kitamura, and M. Teshima, “10-Gbit/s bidirectional and 20-Gbit/s unidirectional 2-ch wireless data transmission system using 120-GHz-band finline orthomode transducers,” *IEICE Trans. Electron.*, vol.E97-C, no.2, pp.101–110, Feb. 2014.
- [10] S. Koenig, D. Lopez-Diaz, J. Antes, F. Boes, R. Henneberger, A. Leuther, A. Tessmann, R. Schmogrow, D. Hillerkuss, R. Palmer, T. Zwick, C. Koos, W. Freude, O. Ambacher, J. Leuthold, and I. Kallfass, “Wireless sub-THz communication system with high data rate,” *Nat. Photonics*, vol.7, no.12, pp.977–981, 2013.
- [11] H. Takahashi, A. Hirata, J. Takeuchi, N. Kukutsu, T. Kosugi, and K. Murata, “120-GHz-band 20-Gbit/s transmitter and receiver MMICs using quadrature phase shift keying,” 2012 7th European Microwave Integrated Circuit Conference, pp.313–316, 2012.
- [12] H. Hamada, H. Nosaka, T. Tsutsumi, H. Sugiyama, H. Matsuzaki, H.-J. Song, G. Itami, T. Fujimura, I. Abdo, and K. Okada, “Millimeter-wave InP device technologies for ultra-high speed wireless communications toward beyond 5G,” 2019 IEEE International Electron Devices Meeting (IEDM), pp.9.2.1–9.2.4, 2019.
- [13] <https://www.rogerscorp.com/advanced-electronics-solutions/rt-duroid-laminates/rt-duroid-5880-laminates>
- [14] F. Parment, A. Ghiotto, T.-P. Vuong, J.-M. Duchamp and K. Wu, “Broadband transition from dielectric-filled to air-filled Substrate Integrated Waveguide for low loss and high power handling millimeter-wave Substrate Integrated Circuits,” 2014 IEEE MTT-S International Microwave Symposium (IMS2014), Tampa, FL, USA, pp.1–3, 2014.
- [15] T. Kumaki, S. Ozeki, A. Hirata, and O. Kagaya, “120-GHz-band Close-Proximity Wireless Communication Using Metamaterial Integrated Glass Substrate,” 2022 IEEE International Workshop on Electromagnetics: Applications and Student Innovation Competition (iWEM), Narashino, Japan, 2022, pp.87–88, 2022.
- [16] D. Kitayama, H.-J. Song, and M. Yaita, “Investigation of plasmon hybridization in split-ring resonators,” 2014 Asia-Pacific Microwave Conference, TH1G-32, 2014.
- [17] X. Cheng, D.E. Senior, J.J. Whalen, and Y.-K. Yoon, “Electrically small tunable split ring resonator antenna,” 2010 IEEE Antennas and Propagation Society Int. Symp., pp.41–44, 2010.
- [18] H. Tao, C.M. Bingham, A.C. Strikwerda, D. Pilon, D. Shrekenhamer, N.I. Landy, K. Fan, X. Zhang, W.J. Padilla, and R.D. Averitt, “Highly flexible wide angle of incidence terahertz metamaterial absorber: Design, fabrication, and characterization,” *Physical Review B*, vol.78, no.24, 2008.
- [19] E.R. Afthar, M.R. Hidayat, and A. Munir, “Analysis of Equivalent Circuit for Bandpass Filter,” The 22nd Asia-Pacific Conference on Communications, pp.361–364, 2016.
- [20] M.K.T. Al-Nuaimi and W.G. Whittow, “Compact Microstrip Band Stop Filter Using SRR and CSSR: Design, Simulation and Results,” European Conference on Antennas and Propagation, pp.2–6, 2010.
- [21] A. Hirata and J. Hirokawa, “Absorber integrated planar slot array antenna for suppression of multiple reflection in 120-GHz-band close-proximity wireless system,” *IEICE Trans. Electron.*, vol.E101-C, no.10, pp.791–800, Oct. 2018.
- [22] K. Itakura, A. Hirata, M. Sonoda, T. Higashimoto, T. Nagatsuma, T. Tomura, J. Hirokawa, N. Sekine, I. Watanabe, and A. Kasamatsu, “Control of 120-GHz-band split ring resonator filter by coupling lattice pattern substrate,” *IEICE Trans. Electron.*, vol.E104-C, no.3, pp.102–111, March 2020.
- [23] A. Hirata, K. Itakura, T. Higashimoto, Y. Uemura, T. Nagatsuma, T. Tomura, J. Hirokawa, N. Sekine, I. Watanabe, and A. Kasamatsu, “Transmission characteristics control of 120 GHz-band bandstop filter by coupling alignment-free lattice pattern,” *IEICE Trans. Electron.*, vol.E104-C, no.10, pp.587–595, Oct. 2021.
- [24] A. Hirata, T. Saijo, Y. Kawamoto, T. Nagatsuma, I. Watanabe, N. Sekine, and A. Kasamatsu, “Evaluation of transmission characteristics of 120-GHz-band close-proximity wireless links using splitting-resonator absorber integrated planar slot antenna,” *IEICE Trans. Electron.*, vol.E106.C, no.9, pp.458–465, 2023.
- [25] K. Itakura, A. Hirata, T. Higashimoto, Y. Uemura, T. Nagatsuma, I. Watanabe, N. Sekine, A. Kasamatsu, “Pass Bandwidth Extension of 120-GHz-Band SRR Filter by Coupling Lattice Pattern Substrate,” International Topical Meeting on Microwave Photonics, Th-P27, Nov. 2020.
- [26] T. Ishibashi, T. Furuta, H. Fushimi, S. Kodama, H. Ito, T. Nagatsuma, N. Shimizu, and Y. Miyamoto, “InP/InGaAs uni-traveling-carrier photodiodes,” *IEICE Trans. Electron.*, vol.E83-C, no.6, pp.938–949, 2000.
- [27] H. Ito, T. Furuta, S. Kodama, and T. Ishibashi, “InP/InGaAs uni-traveling-carrier photodiode with a 310 GHz bandwidth,” *Electron. Lett.*, vol.36, no.21, pp.1809–1810, 2000.
- [28] H. Ito, T. Ito, Y. Muramoto, T. Furuta, and T. Ishibashi, “F-band (90–140 GHz) uni-traveling-carrier photodiode module for a photonic local oscillator,” *Int. Symp. on Space Terahertz Technol.*, pp.318–327, 2010.
- [29] T. Kosugi, M. Tokumitsu, K. Murata, T. Enoki, H. Takahashi, A. Hirata, and T. Nagatsuma, “120-GHz Tx/Rx Waveguide Modules for 10-Gbit/s Wireless Link System,” *IEEE CSIC Symp. Dig.*, pp.25–28, Nov. 2006.
- [30] A. Hirata, T. Kosugi, H. Takahashi, J. Takeuchi, K. Murata, N. Kukutsu, Y. Kado, S. Okabe, T. Ikeda, F. Suginosita, K. Shogen, H. Nishikawa, A. Irino, T. Nakayama, and N. Sudo, “5.8-km 10-Gbps data transmission over a 120-GHz-band wireless link,” 2010 IEEE International Conference on Wireless Information Technology and Systems (ICWITS), 2010.



Tomohiro Kumaki received his B.S. degrees in engineering in 2022 from Chiba Institute of Technology, Chiba, Japan, where he is currently working toward the M.S. degree with the Graduate School of Engineering. Mr. Kumaki is a student member of IEICE.



Akihiko Hirata received his B.S. and M.S. degrees in chemistry and his Dr. Eng. degree in electrical and electronics engineering from Tokyo University, Tokyo, Japan, in 1992, 1994, and 2007, respectively. He joined the Atsugi Electrical Communications Laboratories of Nippon Telegraph and Telephone Corporation (presently NTT Device Technology Laboratories) in Kanagawa, Japan, in 1994. He was a senior research engineer and supervisor at NTT Device Technology Laboratories. He has been a professor at the

Chiba Institute of Technology since 2016. His current research involves millimeter-wave antennas and ultra-broadband millimeter-wave wireless systems. Prof. Hirata is a senior member of IEEE and a senior member of IEICE.



Tsubasa Saijo received the B.S. degree in engineering science in 2020 from Osaka University, Osaka, Japan, where he is currently working toward the M.S. degree with the Graduate School of Engineering Science. His research focuses on the secure wireless communication by combining terahertz and optical waves.



Yuma Kawamoto received the B.S. degree in engineering science in 2020 from Osaka University, Osaka, Japan, where he is currently working toward the M.S. degree with the Graduate School of Engineering Science. His research focuses on the integration and packaging of THz devices for wireless communications. Mr. Kawamoto is a student member of IEICE.



Tadao Nagatsuma received his B.S., M.S., and Ph.D. degrees in electronic engineering from Kyushu University, Fukuoka, Japan, in 1981, 1983, and 1986, respectively. In 1986, he joined the Electrical Communications Laboratories, Nippon Telegraph and Telephone Corporation (NTT), Atsugi, Kanagawa, Japan. From 1999 to 2002, he was a Distinguished Technical Member with NTT Telecommunications Energy Laboratories. From 2003 to 2007, he was a Group Leader with NTT Microsystem Integra-

tion Laboratories and was an NTT Research Professor from 2007 to 2009. Since 2007, he has been with Osaka University, Osaka, Japan, where he is currently a Professor with the Division of Advanced Electronics and Optical Science, Department of Systems Innovation, Graduate School of Engineering Science. His research interests include ultrafast electronics and millimeter-wave and terahertz photonics. Dr. Nagatsuma is a Fellow of the IEEE, and a Fellow of the Institute of Electronics, Information and Communication Engineers (IEICE), Japan. He currently serves as an Associate Editor of the IEEE Photonics Technology Letters and the IEEE Trans. Terahertz Science and Technology, and a President of the Terahertz Systems Consortium and a Past-Vice President of the IEICE. He was the recipient of numerous awards including the 1989 IEICE Young Engineers Award, the 1992 IEEE Andrew R. Chi Best Paper Award, the 1997 Okochi Memorial Award, the 1998 Japan Microwave Prize, the 2000 Ministers Award of the Science and Technology Agency, the 2002 and 2011 Asia-Pacific Microwave Conference Prize, the 2004 YRP (Yokosuka Research Park) Award, the 2006 Asia-Pacific Microwave Photonics Conference Award, the 2006 European Microwave Conference Prize, the 2007 Achievement Award presented by the IEICE, the 2008 Maejima Award, the 2011 Recognition from Kinki Bureau of Telecommunications, Ministry of Internal Affairs and Communications, the 2011 Commendation for Science and Technology by the Ministry of Education, Culture, Sports, Science and Technology, and the 2014 IEEE Tatsuo Ito Award, and the 2020 Distinguished Achievement and Contributions Award by the IEICE.



Osamu Kagaya received the B.S. and M.E. and D.E. degrees in engineering from the Tokyo University of Agriculture and Technology (TUAT), Tokyo, Japan, in 1999, 2002 and 2022, respectively. He joined AGC Inc. in 2001. Since then, he has been engaged in research on glass antennas and electromagnetic scattering.